Supplementary Information

"Identification and characterization of a bacterial hydrosulfide ion channel"

Bryan K. Czyzewski and Da-Neng Wang

Supplementary Table 1. Thermostabilization of HSC protein by various anions

Condition	Apparent T_m (°C) [a]
Control	53.3 ± 0.1
Na_2SO_3	53.8 ± 0.3
$NaHCO_2$	57.1 ± 0.2
NaCl	57.3 ± 0.4
$NaNO_2$	58.5 ± 0.2
NaHS	61.7 ± 0.3

[a]: T_m was determined by fitting the peak heights from size exclusion chromatography fitted to a Boltzman sigmoidal curve.

Supplementary Table 2. Crystallographic data collection and refinement statistics (molecular replacement)

	Wild Type pH 9.0	**Wild Type** pH 7.5	**Wild Type** pH 4.5	**K16S**	**L82V**	**T84A**	**K148E**	**F194I**
Data collection								
Space group	$P2_12_12_1$	$P2_1$	$C222_1$	$P2_12_12_1$	$P2_12_12_1$	$P2_12_12_1$	$P2_12_12_1$	$P2_12_12_1$
Cell dimensions								
a, *b*, *c* (Å)	98.8, 119, 150	95.9, 102, 168	121,163,194	98.7, 119, 151	99, 119, 151	99, 118, 151	99.4, 118, 151	98.6, 118, 150
a, *b*, *g* (°)	90, 90, 90	90, 90.2, 90	90, 90, 90	90, 90, 90	90, 90, 90	90, 90, 90	90, 90, 90	90, 90, 90
Resolution (Å)	50-2.2 (2.24-2.2)*	50-3.2 (3.26-3.2)*	50-3.0 (3.05-3.0)*	50-2.3 (2.34-2.3)*	50-2.5 (2.54-2.5)*	50-2.4 (2.44-2.4)*	50-2.1 (2.14-2.1)*	50-2.03 (2.07-2.03)*
R_{sym} or R_{merge}	7.8 (89.8)	6.1 (56.3)	13.8(70.7)	13.3 (80.4)	10.4 (73.3)	9.1 (80.3)	10.5 (69.3)	9.3, (77.1)
I / σ(I)	40.2 (3)	19.9 (2.1)	14.3 (2.3)	24.3 (2.8)	30.2 (3.3)	24.3 (2.2)	30.5 (3.5)	35.1, (2.8)
Completeness (%)	99.9 (100)	98.8 (97.2)	99.9 (98.5)	99.9 (99.9)	99.9 (100)	99.2 (98.8)	99.9 (100)	99.7 (100)
Redundancy	9.7 (9.5)	3.4 (3.1)	7.1 (6.9)	7.1 (5.9)	7.7 (7.6)	6.8 (6.4)	7.1 (7.0)	7.3 (7.5)
Refinement								
No. reflections	871,616	181,002	273,460	560,983	915,038	472,750	745,180	845,091
R_{work} / R_{free}	18/21.1	19.3/25.3	18.6/24	18.5/23	16.2/0.21	21.3/27.5	16.8/19.9	17.4/20.1
No. atoms	10,307	19,009	9,787	10,419	10,111	9,941	10,315	10,356
Protein	1,294	2,588	1,281	1,293	1,293	1,293	1,293	1,294
Ligand	225	93	120	225	105	92	120	212
Chloride	-	-	-	-	5	-	-	-
Zinc	-	-	5	-	-	-	-	-
Water	198	84	36	336	301	172	433	300
B-factors	64	103.9	59.2	44.4	58.9	62.2	39.3	49.5
Protein	63.2	97.3	52.5	41.1	57.9	62.1	52.5	49.2
Ligand	102.1	106.3	97.7	88.1	82.5	87.4	97.7	92
Water	58.6	55.0	32.8	45.1	66.7	53.0	32.8	51.4
Chloride	-	-	-	-	59.4	-	-	-
Zinc	-	-	67.9	-	-	-	-	-
R.m.s. deviations								
Bond lengths (Å)	0.007	0.008	0.005	0.007	0.008	0.014	0.011	0.009
Ramachandran statistics (%)								
Favored	97.6	86	96.9	97.2	97	92.6	97.3	97.2
Outliers	0.5	0.2	0.9	0.6	0.3	1.4	0.2	0.7

Notes: *: A single crystal was used for each structure. **: $R_{sym} = \Sigma|I_j - \langle I_j \rangle|/\Sigma I_j$, where $\langle I_j \rangle$ is the averaged intensity for symmetry related reflections. Redundancy represents the ratio between the number of measurements and the number of unique reflections. *R* factor = $\Sigma|F(obs) - F(cal)|/\Sigma F(obs)$; 5% of the data that were excluded from the refinement were to calculate R_{free}. The average *B* factor was calculated for all non-hydrogen atoms. r.m.s.d. of bond is the root-mean-square deviation of the bond angle and length. Numbers in parentheses are statistics of the highest resolution shell.

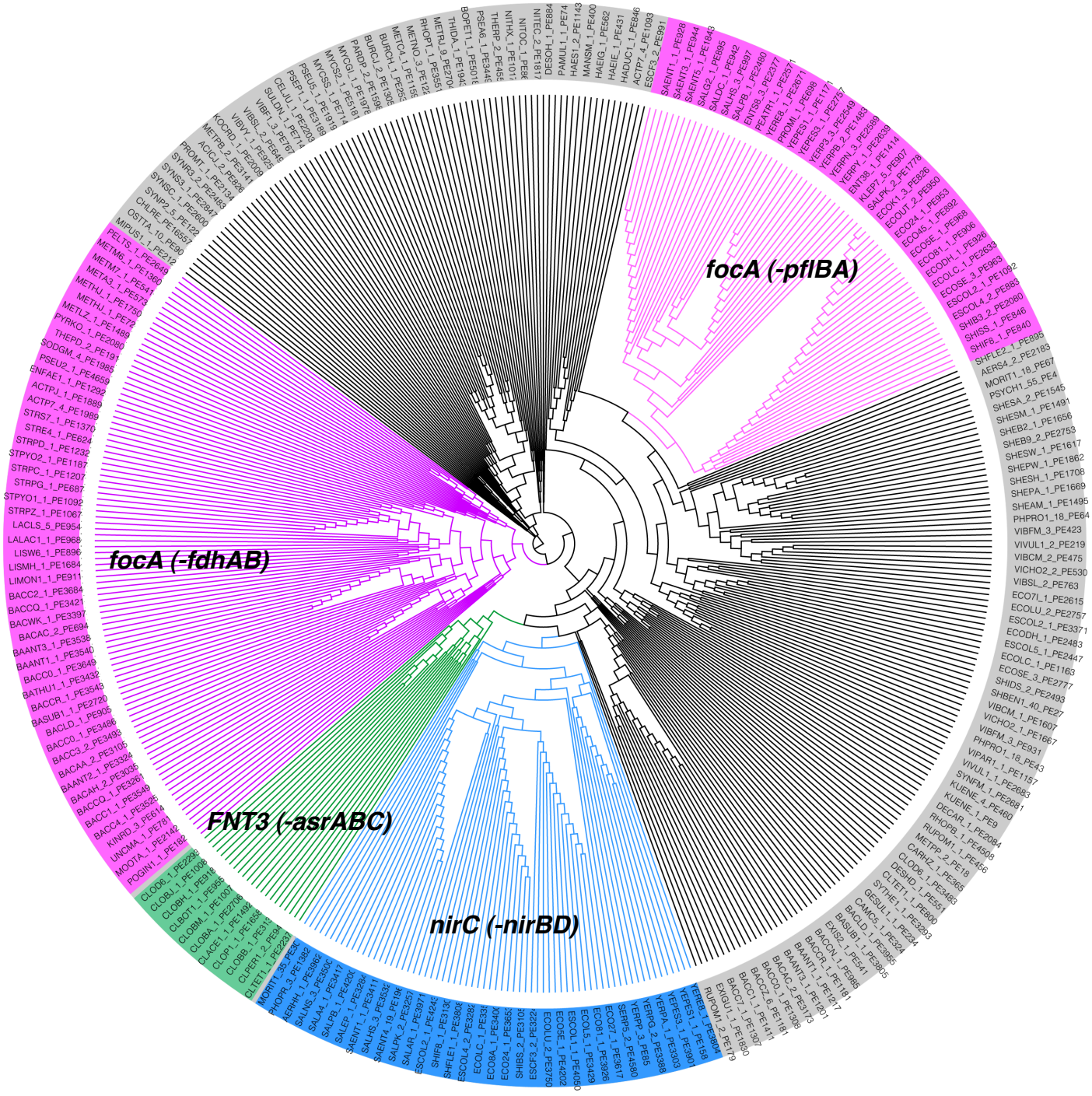

Supplementary Figure 1. Phylogenetic tree of bacterial and archaeal FNT family members. Branches are colored based on genetic linkage to metabolic enzymes: genes linked to pyruvate formate lyase (*pflBA*) in bacteria or formate dehydrogenase (*fdhAB*) in archaea are colored pink, genes linked to nitrite reductase (*nirBD*) are colored blue, and genes linked to sulfite reductase (*asrABC*) are colored green. These genes are predicted to encode for channel proteins. The species and uniprot accession numbers for 158 of the 474 analyzed members are displayed.

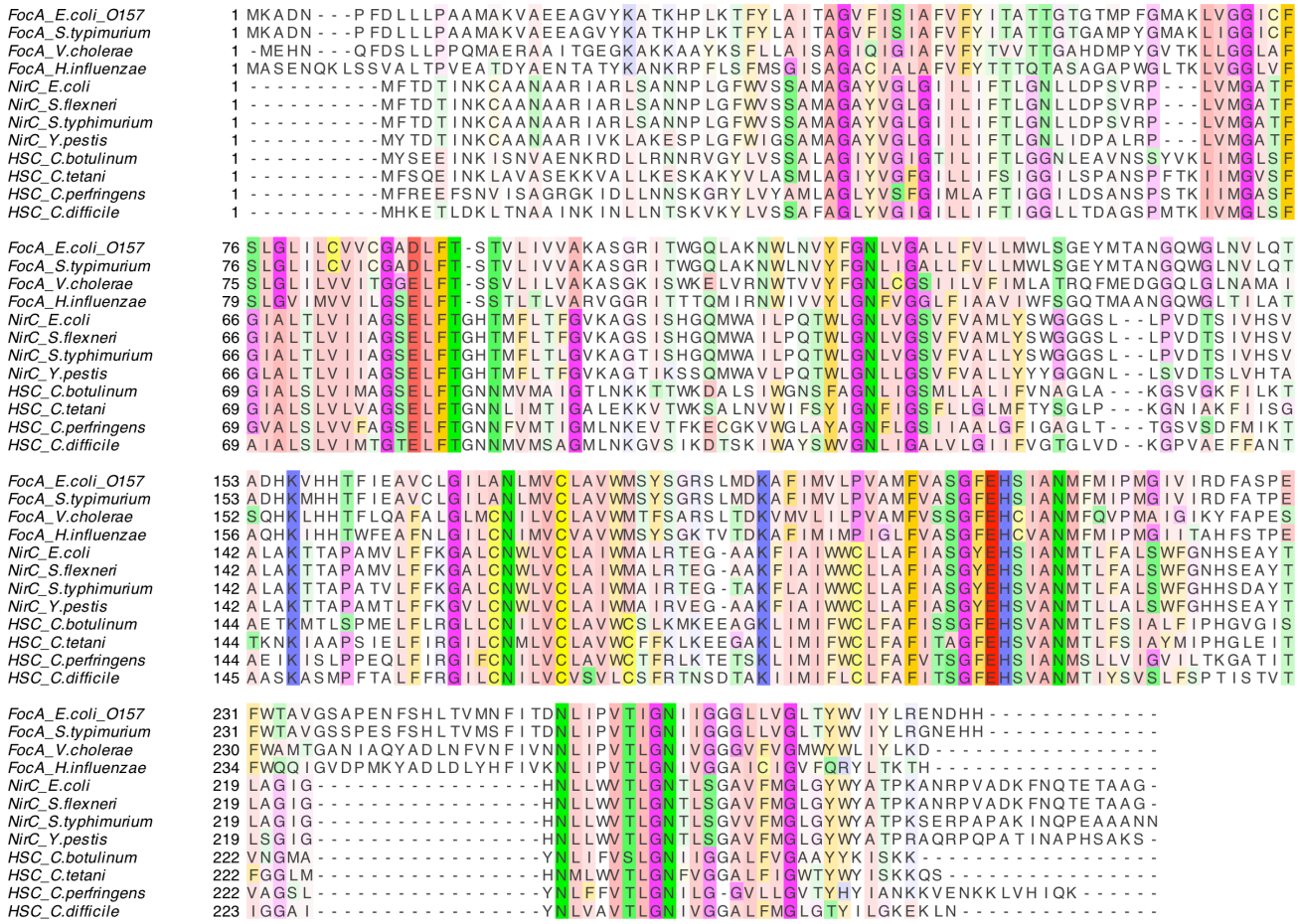

Supplementary Figure 2. Amino acid sequence alignment of FocA, NirC and FNT3/HSC members of the FNT channel family. Alignment was generated using Jalview and colored by the Taylor convention of residue properties and conserved sequence identity.

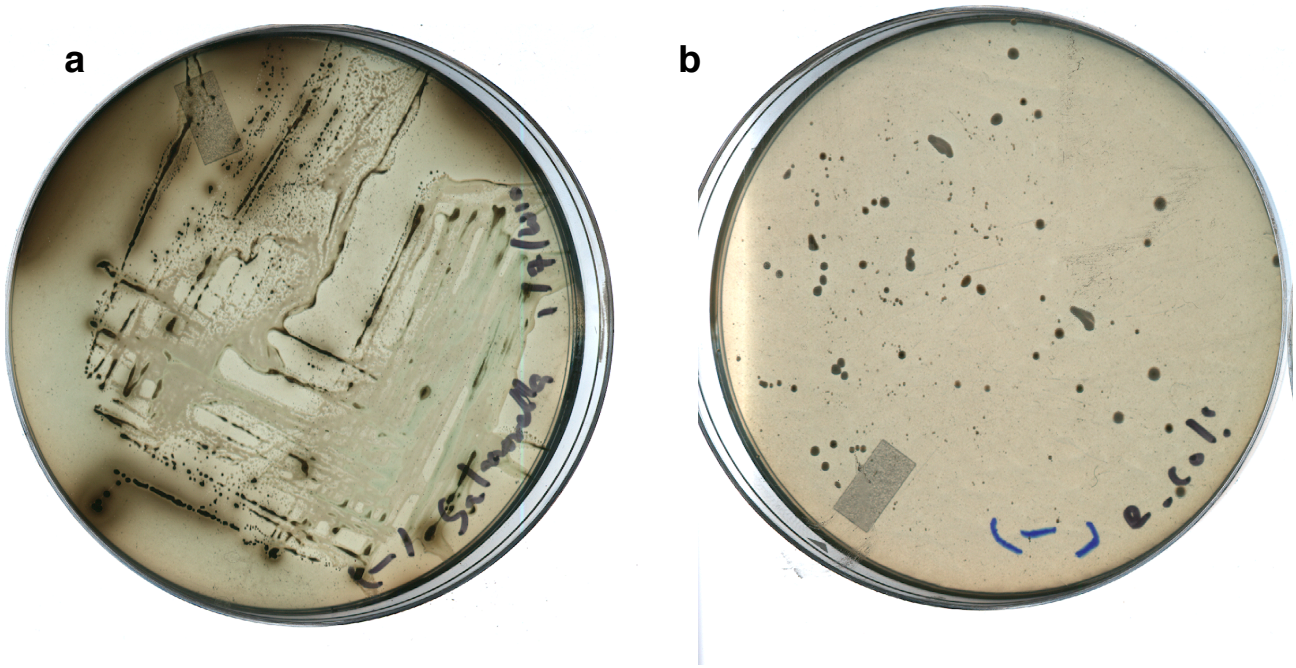

Salmonella typhimurium	
Growth	+++
Sulfide Gas	+++

Escherichia coli	
Growth	+
Sulfide Gas	-

Supplementary Figure 3. Bismuth sulfite agar assay for the detection of hydrogen sulfide production. a, Positive control in *Salmonella typhimurium* possesses a sulfate reductase operon. Growth was observed and sulfide gas production was visualized by a darkening at the edge of the colonies and in the surrounding agar. **b**, Negative control in *Escherichia coli* does not contain a sulfate reductase operon.

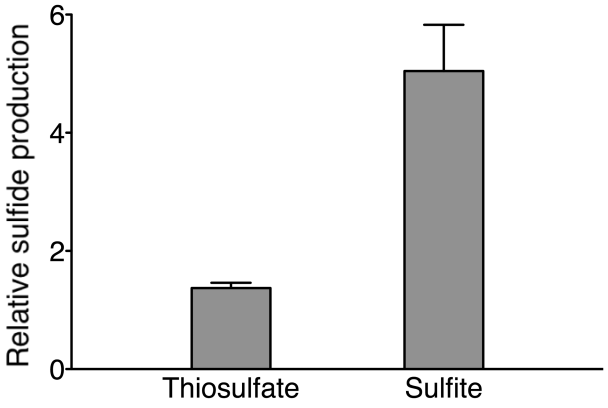

Supplementary Figure 4. Bacterial whole-cell assay for hydrosulfide transport. Relative fold increase in sulfide production of vector-transformed versus *FNT3/HSC*-transformed *Salmonella typhimurium* is shown. The levels of sulfide produced and exported by the *Salmonella typhimurium* were measured in the media supplemented with either thiosulfate or sulfite.

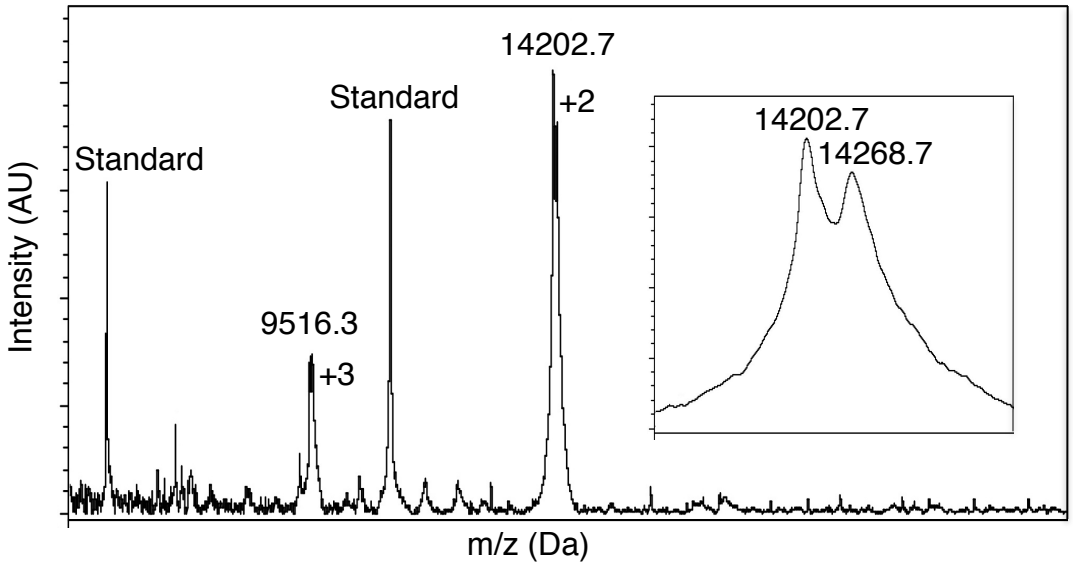

Supplementary Figure 5. Mass measurements of purified HSC protein using MALDI-TOF mass spectrometry. The expected mass for HSC is 28537.8 Da. The doubly-charged +2 ions show two peaks, at 28535.4 Da and 28403.4 Da, respectively, indicating partial cleavage of the N-terminal methionine.

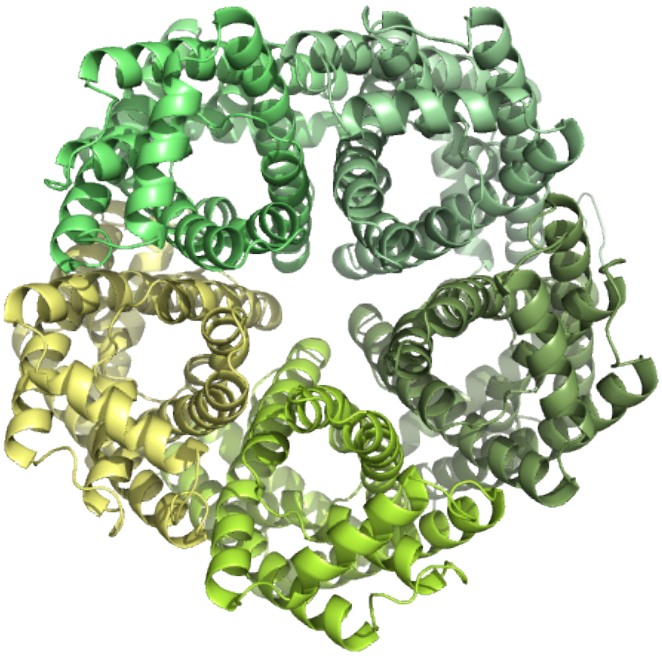

Supplementary Figure 6. Structure of the HSC pentamer determined from the high pH crystal form (pH 9.0). The 2.2 Å resolution structure is shown as viewed from the periplasmic side. The structures of the five HSC protomers are identical.

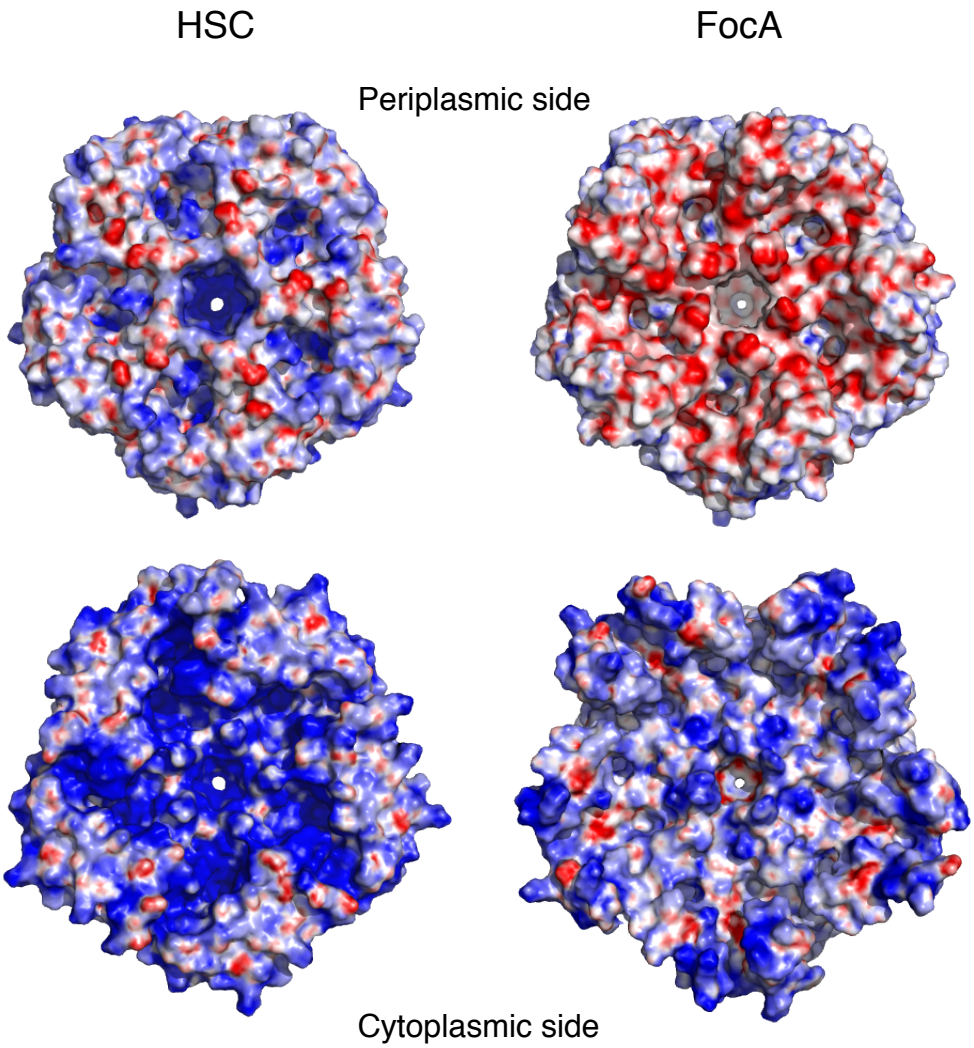

Supplementary Figure 7. Comparison of electrostatic surface properties of HSC and FocA from *V. cholerae*. Electrostatic surface representations were generated in Pymol using the APBS plugin with a -20 to 20 kT/e^- electrostatic potential. The cytoplasmic surface of HSC is highly positive, which helps to attract HS^- ions.

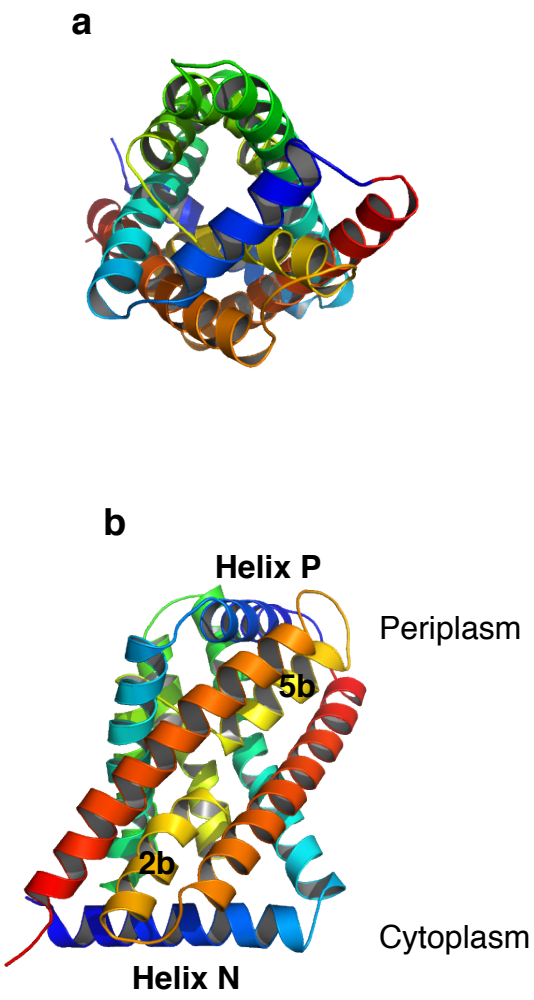

Supplementary Figure 8. Structure of HSC protomer of the high pH form (pH 9.0). a, Viewed from the periplasmic side. **b**, Viewed from within the membrane plane. The N- and C-terminal halves of the protein are colored in a double-rainbow scheme to show sequence homology and the twofold inverted symmetry.

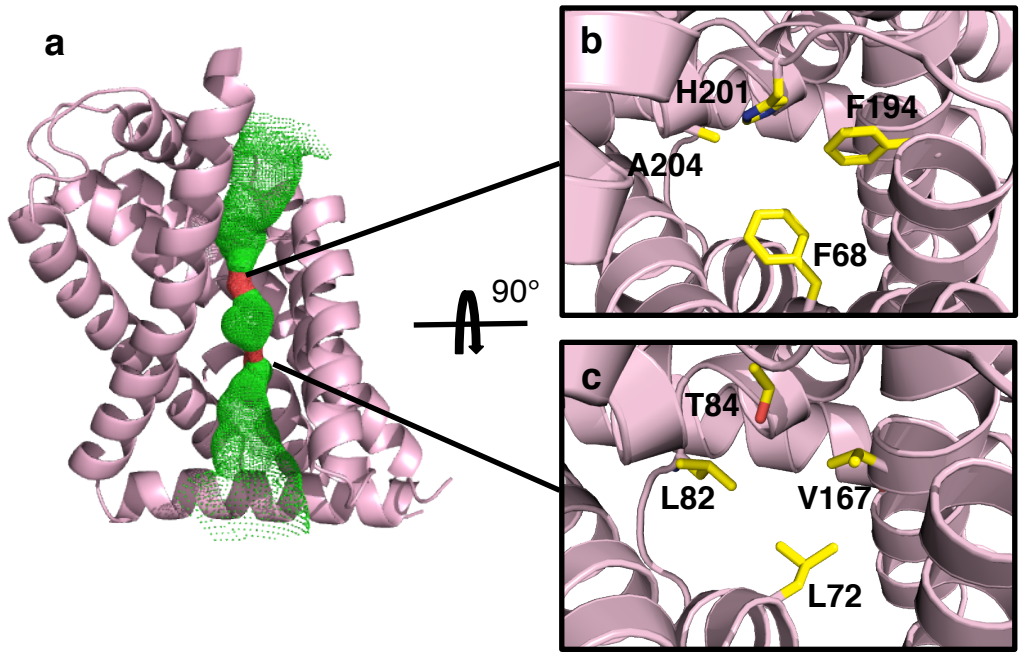

Supplementary Figure 9. Pore structure of HSC. a, Structure of an HSC protomer superimposed with the pore calculated using HOLE. The pore is colored to indicate the radius of water, where green is permeable to water and red is impermeable. Transmembrane helix TM2 has been removed for clarity. **b**, The central constriction ring. **c**, The cytoplasmic constriction slit. **b** & **c** are viewed from the periplasm.

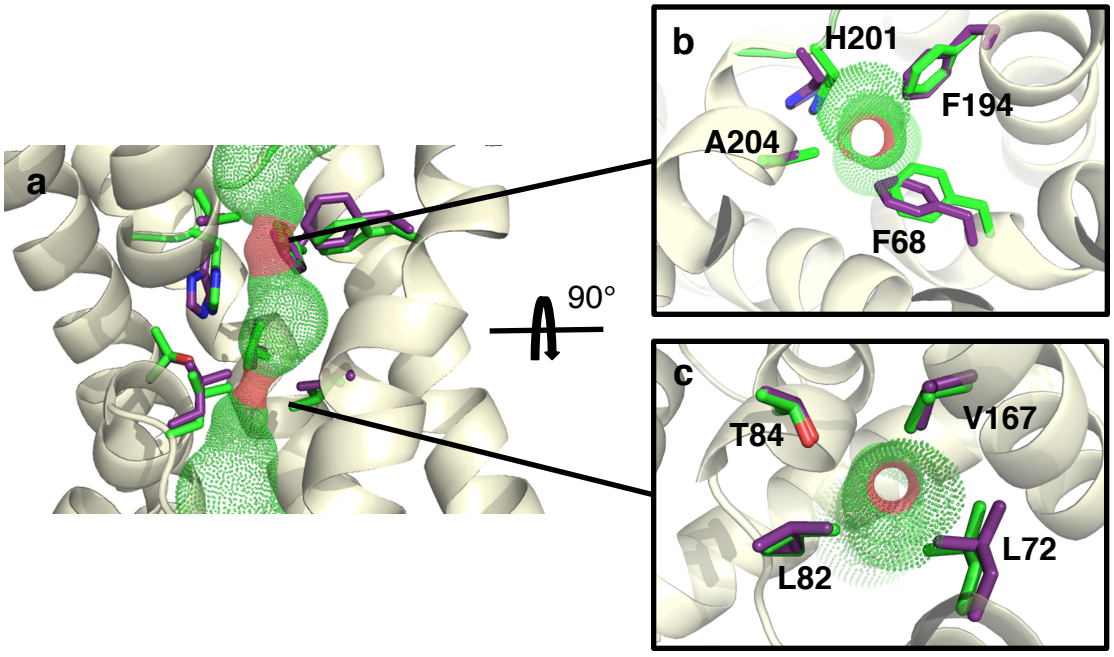

Supplementary Figure 10. Comparison of the selectivity filters of HCS and of *Vibrio cholerae* FocA. Residues at the selectivity filter of HSC (green) are superimposed with those equivalent from FocA (purple). **a**, Side view. **b**, The central constriction ring. **c**, The cytoplasmic constriction slit. **b** & **c** are viewed from the periplasm.

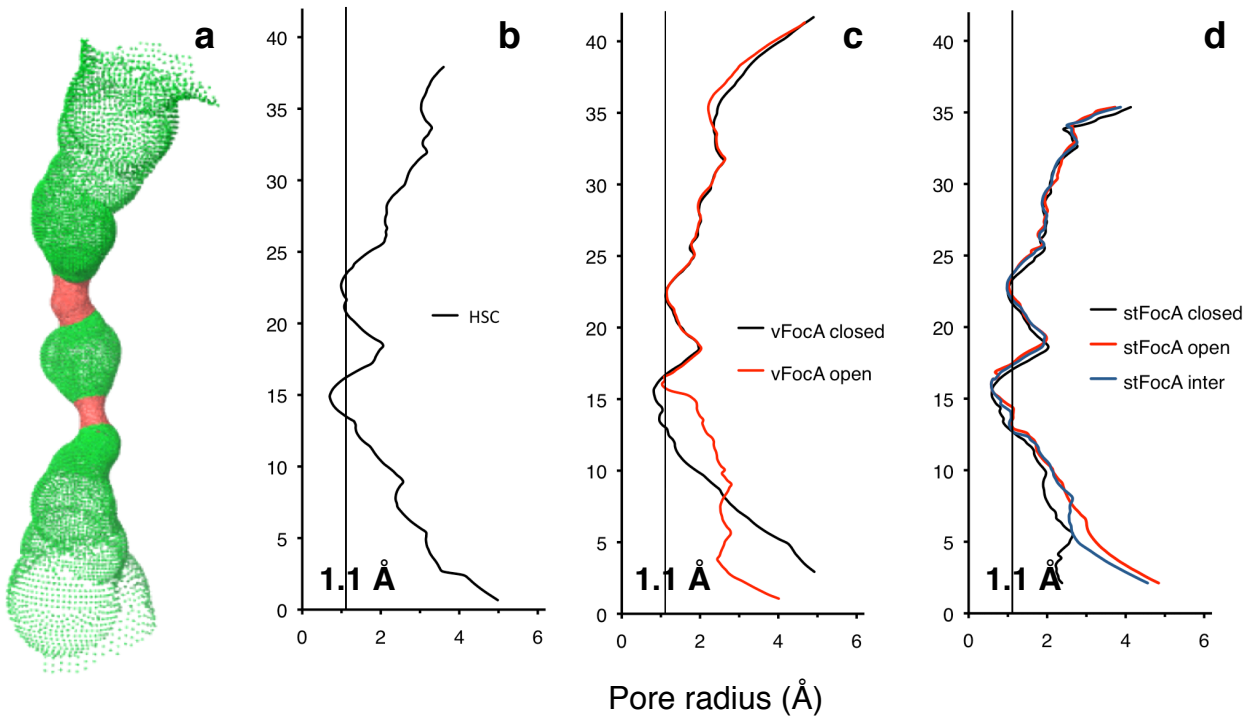

Supplementary Figure 11. Comparison of pore radii of HSC and FocA channels. **a**, Pore of HSC calculated from HOLE. Red colored constrictions are impermeable to water while green colored regions are wide enough to allow water to pass. **b**, Pore radius of *Clostridium difficile* HSC. The channel is in its closed state. **c**, Pore radius of *Vibrio cholerae* FocA (PDB 3KLZ) in both closed (black line) and open (red line) states. **d**, Pore radius of *Salmonella typhimurium* FocA (3Q7K) in closed (black line), open (red line) and intermediate (blue line) states, as defined by Lu *et al.* [16]. The radius of 1.1 Å is typically regarded as the boundary of an open and a closed state for water channels.

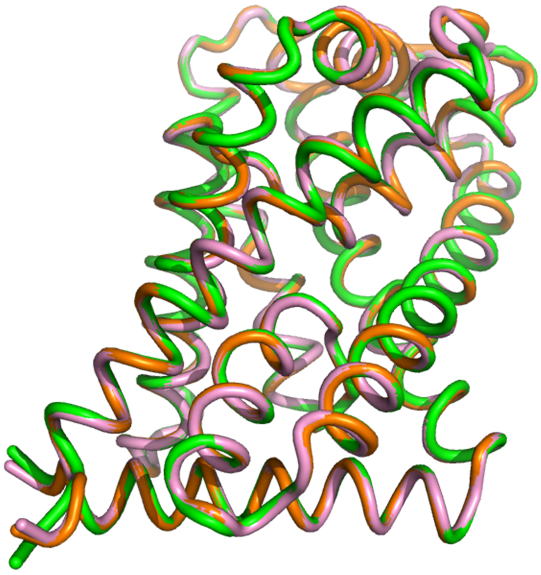

Supplementary Figure 12. Structure comparison of HSC at various pHs. Backbone superimposition is shown of the HSC crystal structures from high pH (pH 9.0, orange), neutral pH (pH 7.5, pink) and low pH (pH 4.5, green). The three crystal structures are nearly identical.

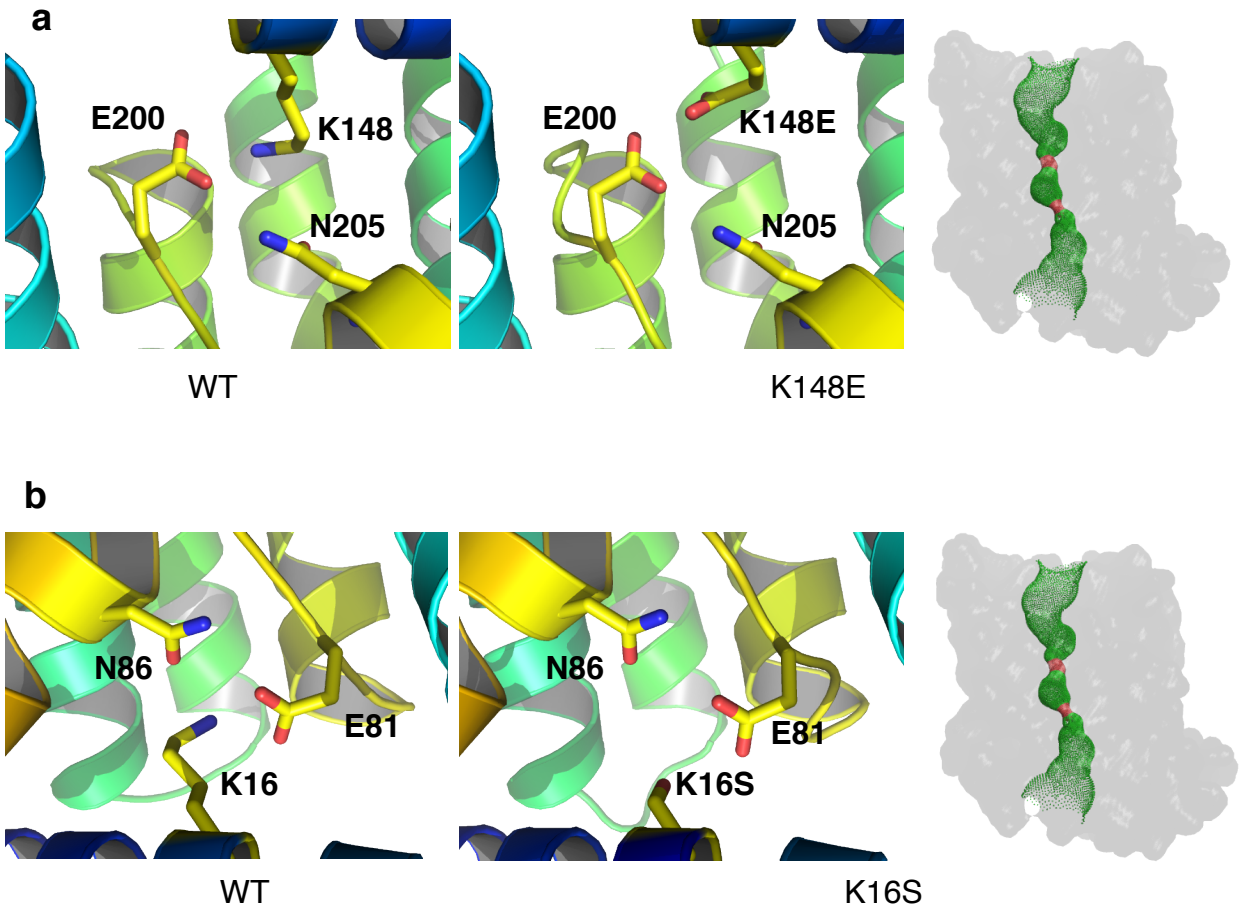

Supplementary Figure 13. Comparison of the wild-type HSC structure with those of salt-bridge-triad mutants. a, Upper triad structures of the wild-type and of the K148E mutant. **b**, Lower triad structures of the wild-type and of the K16S mutant. Neither mutation, although each disrupted its respective salt-bridge, caused conformational changes that opened the channel, as shown in the HOLE calculations.

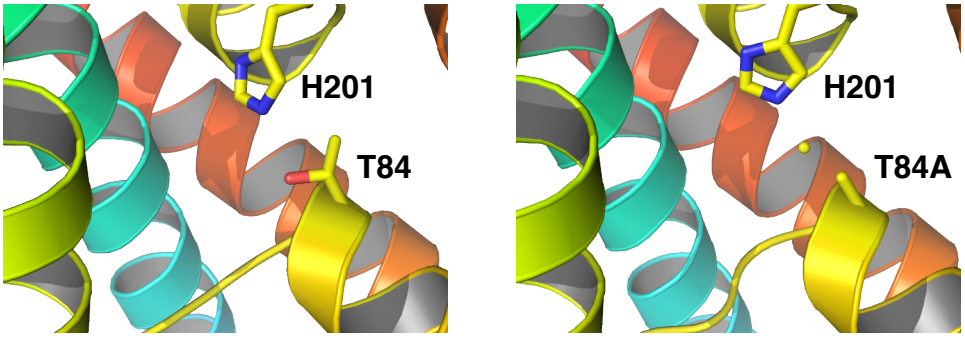

Supplementary Figure 14. Comparison of the wild-type HSC structure with that of the Thr84Ala mutant. The mutation's disruption of the His201-Thr84 hydrogen bond did not cause large-scale conformational change of the protein to open the channel. The equivalent hydrogen bond between conserved residues in the *Vibrio cholerae* FocA is believed to be important for the gating mechanism of that channel by formate concentration.